# Direct estimation of forest aboveground biomass from UAV LiDAR and RGB observations in forest stands with various tree densities

# Direct estimation of forest aboveground biomass from UAV LiDAR and RGB observations in forest stands with various tree densities

BY KANGYU SO, BS

A thesis submitted to the School of Graduate Studies in Partial Fulfillment of the Requirements for the Degree Master of Earth and Environmental Science

MASTER OF EARTH AND ENVIRONMENTAL SCIENCE (2025)

McMaster University, Hamilton, Ontario, Canada

TITLE: Direct estimation of forest aboveground biomass from UAV LiDAR and RGB observations in forest stands with various tree densities

AUTHOR: Kangyu So, BS (McMaster University, 2025)

SUPERVISOR: Professor Alemu Gonsamo

NUMBER OF PAGES: iii, 43

**Lay Abstract**

The effects of forest thinning practices on biomass regeneration are not well understood as traditional field methods for measuring forest characteristics are costly and impractical for large spatial extents. To monitor and report on biomass components more effectively, we used unoccupied aerial vehicle (UAV) imagery and laser scanning observations, segmentation algorithms, and a deep learning predictive model, for a 14-ha mixed forest stand in Southern Ontario. Laser scanning observations were segmented into tree crowns for the deep learning model, and the crown size, height, and biomass of individual trees were output from UAV imagery. Our results indicate that a combined segmentation and modelling approach can provide accurate estimates of biomass components in forests, even under conditions where their stand density and spatial patterns are manipulated.

**Abstract**

Canada's vast forests play a substantial role in the global carbon balance but require laborious and expensive forest inventory campaigns to monitor changes in aboveground biomass (AGB). Light detection and ranging (LiDAR) or reflectance observations onboard airborne or unoccupied aerial vehicles (UAV) may address scalability limitations associated with traditional forest inventory but require simple forest structures or large sets of manually delineated crowns. Here, we introduce a deep learning approach for crown delineation and AGB estimation reproducible for complex forest structures without relying on hand annotations for training. Firstly, we detect treetop and delineate crowns with LiDAR point cloud using marker-controlled watershed segmentation (MCWS). Then we train a deep learning model on annotations derived from MCWS to make crown predictions on an UAV red, blue and green (RGB) tiles. Finally, we estimate AGB metrics from tree height and crown diameter-based allometric equations, all derived from UAV data. We validate our approach using a 14-ha mixed forest stands with various experimental tree densities in Southern Ontario, Canada. Our results demonstrate an 18% improvement in AGB estimation accuracy when the unsupervised LiDAR only algorithm is followed by a self-supervised RGB deep learning model. In unharvested stands, the self-supervised RGB model performs well for height ($R^2$=0.79) and AGB ($R^2$= 0.80) estimation. In thinned stands, the performance of both unsupervised and self-supervised methods varied with stand density, crown clumping, canopy height variation, and species diversity. These findings suggest that MCWS can be supplemented with self-supervised deep learning to directly estimate biomass components in complex forest structures as well as atypical forest conditions where stand density and spatial patterns are manipulated.

**Keywords:** LiDAR, UAV, biomass, unmanned aerial vehicle, crown delineation, self-supervised deep learning

**Acknowledgements**

I would like to first acknowledge my advisor Dr. Alemu Gonsamo, whose feedback, expertise, and continuous support were integral to the completion of this thesis. I would also like to thank my committee members Dr. Darren Scott and Dr. Jiaxin Chen, as well as my co-authors Jenny Chau, Dr. Derek T. Robinson, Sean Rudd, and Dr. Dominic Cyr for their contributions to the research. Finally, I am grateful for the support that all of my friends and colleagues in the McMaster Remote Sensing Laboratory has given me throughout my Master's. This research was funded by the Natural Sciences and Engineering Research Council of Canada (NSERC) Alliance Grant (RGPIN-2020-05,708), and Environment and Climate Change Canada (ECCC) Grants and Contributions program (GCXE24S085).

**Table of Contents**

**List of Tables**

**List of Figures**

**List of Abbreviations and Symbols**

| | |
|---|---|
| 33A | 33% Aggregate crown retention |
| 33D | 33% Dispersed crown retention |
| 55A | 55% Aggregate crown retention |
| 55D | 55% Dispersed crown retention |
| AGB | Aboveground biomass |
| ANOVA | Analysis of variance |
| C | Carbon |
| CHM | Canopy height model |
| CON | Unharvested control |
| DBH | Diameter at breast height |
| DEM | Digital elevation model |
| LAI | Leaf area index |
| LiDAR | Light detection and ranging |
| MCWS | Marker-controlled watershed segmentation |
| $PPFD_U$ | Photosynthetic photon flux density at the understory |
| RGB | Red, blue and green |
| UAV | Unoccupied aerial vehicles |
| TWI | Topographic Wetness Index |

# Chapter 1: LiDAR and RGB-based Methods to Estimate Biomass

## *1.1 Introduction*

Forests are essential to global Earth-system health and carbon (C) cycling through several ecosystem functions, including C sequestration and storage (Martire et al., 2015). Forests are critical terrestrial sinks for atmospheric $CO_2$ due to their ability to store large amounts of C in trees and forest soils. Canada has one of the largest contiguous forest ecosystems on Earth, spanning an area of 4 million km$^2$ (Gonsamo & Chen, 2011). Canada's forests store 20.9 Pg C in their biomass, around 6.5% – 7.2% of the total C stored in AGB in all forests on Earth (Sothe et al., 2022). With 2.06 million km$^2$ of Canada's forests covered under a management plan that includes timber production and conservation, frequent monitoring of changes in tree aboveground biomass (AGB) is necessary for developing climate change mitigation solutions. Traditionally, AGB is estimated from allometric equations that use in-situ tree height and diameter at breast height (DBH) measurements. Height and DBH-based allometric equations are available for 33 common tree species in Canada, adjusted for interspecies variations in biomass compartments such as bark, branches, foliage, and wood (Lambert et al., 2005). However, traditional national forest inventories target a limited number of commercial species and growing conditions, and obtaining consistent field measurements for forest monitoring is costly and impractical for large spatial extents of forests which have great variety in species mix and growing conditions (Iglhaut et al., 2019; Pappas et al., 2022).

Advancements in remote sensing enable consistent monitoring and reporting on forest characteristics through aerial and satellite-based forest inventories (Xu et al., 2021). Compared to traditional forest inventory procedures that involve manual ground-based measurements, aerial remote-sensing-based forest inventories, collected by unoccupied aerial vehicles (UAV), can provide relatively better spatial and temporal coverage using red, green and blue (RGB) imagery or light detection and ranging (LiDAR) data (White et al., 2016). LiDAR can generate 3-dimensional point clouds, which provide location and structural information of tree biomass components (Xu et al., 2021). Although RGB and LiDAR data are most commonly and efficiently collected through UAVs or satellites, as of yet, they are unable to provide sufficiently accurate DBH measurements that are typically used to estimate AGB. Thus, traditional allometric equations for AGB estimation are unsuitable for UAV-based inventories and would need to be adapted. Previous studies have proposed methods to approximate DBH from crown diameter for existing allometric equations or develop equations to estimate AGB directly from crown diameter (Jucker et al., 2022). Adapting DBH-based allometric equations to crown-based equations offers significant practical benefits since developing new equations from crown measurements to estimate AGB necessitates direct biomass sampling of trees, a method that is both destructive and impractical for large spatial scales (Dalponte & Coomes, 2016; Kim et al., 2010; Ni-Meister et al., 2010).

Small-footprint airborne laser scanning methods are proliferating as an approach for extracting forest inventory data from LiDAR point clouds. The point cloud can be used to generate a canopy height model (CHM), which can subsequently be analyzed to estimate individual treetop's location and height (e.g., local maximum filtering, Panagiotidis et al. (2016)). Treetop locations can be used as markers in a watershed segmentation (e.g., Yun et al. (2021)), which is a boundary detection-based technique that has successfully delineate tree crowns (i.e., segments) in a CHM (e.g., Yin and Wang (2019)). Marker-controlled watershed segmentation (MCWS) is a variant of the method that uses an inverted CHM to treat treetops as individual catchment basins for a pouring water algorithm. Water is poured until it reaches the highest point of a basin, and the resulting edges delineate the crown profiles (Yun et al., 2021). While commonly used to generate forest inventory data, MCWS-based crown delineation is limited in forests with minimal tree height variance and high crown clumping (Yin & Wang, 2019). Yet, the impact of forest structural complexity on MCWS crown delineation has not been rigorously assessed, particularly in the context of forests under a management plan with various silvicultural treatments. Region-growing segmentations are an alternative method for crown delineation that uses a decision tree method to grow individual crowns around treetops (Dalponte & Coomes, 2016). Improved tree detection and crown segmentation has been achieved using deep learning and region-growing algorithms, but training datasets are limited to small forests with very high point density LiDAR data (e.g., 1000 points/m$^2$, Wielgosz et al. (2024)). Additionally, some models require terrestrial or mobile laser scanning data to separate individual trees in the point clouds, which limits reproducibility for larger study areas where only airborne laser scanning may be available (Wielgosz et al., 2024).

Deep learning neural networks for crown delineation using RGB-band mosaics have been gaining traction in recent years. Current models primarily use either a mask region-based or U-Net convolutional neural network, which require large sets of ground truth information for training (Freudenberg et al., 2022; Hao et al., 2021). Over large study areas, models are trained on manually delineated crowns, with high agreement between hand annotations in the test data and the model predictions. These methods require manual intervention or large sets of hand annotations for individual tree crown analysis in dense forest canopies common in Canadian forests (Brandt et al., 2020; Leckie, 2003). LiDAR crown prediction has been explored as an alternative to manual delineation for training data. Weinstein et al. (2019) developed a segmentation model trained on trees generated from unsupervised LiDAR algorithms, with moderate crown precision and recall in simple forest structures. While this self-supervised method enables automated segmentation, there is a limited understanding of its application for predicting forest inventory (Weinstein et al., 2019). Furthermore, the open-source model has yet to be trained on Canadian forests, particularly for sites under silvicultural thinning treatments with variable forest structures (Weinstein et al., 2020).

Here, we investigate the accuracy of unsupervised LiDAR and self-supervised RGB forest inventory predictions in a 14-ha northern temperate coniferous forest stand in Canada (So et al., 2024). We used a combination of UAV LiDAR and RGB data acquired during leaf-on and leaf-off conditions, MCWS, and open-source deep learning models to generate tree height and crown diameter predictions of a forest stand undergoing various thinning treatments. We also developed crown-based allometric equations from existing forest inventory databases to estimate AGB from ground truth data, unsupervised LiDAR and self-supervised RGB predictions. Through this work, we demonstrate a self-supervised method for height and crown estimation that is reproducible for forests of varying structural complexities and help estimate AGB directly from remote sensing data.

### *1.2 Materials and Methods*

#### *1.2.1 Site Description*

We carried out the study at a 14-ha temperate red pine (*Pinus resinosa*) plantation stand located in the St. Williams Conservation Reserve (42.704444 N, 80.358056 W). The study site is located approximately 3 km north of Lake Erie in southern Ontario and belongs to the larger Turkey Point Observatory (Zugic et al., 2021). Managed by the Ontario Ministry of Natural Resources, the stand was planted in 1931 with red pine seedlings placed 2 meters apart in furrowed rows. The stand density was reduced from ~2500 trees/ha to ~1875 trees/ha in 1960 through forest thinning. In 2014, the ministry divided the study site into 14 1-ha plots and applied one of five variable retention harvesting (VRH) treatments (unharvested control (CON), 33% aggregate crown retention (33A), 55% aggregate crown retention (55A), 33% dispersed crown retention (33D), 55% dispersed crown retention (55D)) (Fig. 1). VRH are silvicultural treatments that manipulate the spatial distribution of residual forest stands into evenly spread (dispersed) or clustered (aggregate) patterns after harvest. The treatments focus on preserving forest structural complexity to enhance stand regeneration and biomass growth rate (So et al., 2024). Treatment parameters were applied using provincial guidelines on shelterwood system regeneration of red and white pine forests (Table 1) (So et al., 2024; Zugic et al., 2021). Tree clumping is retained at base level in unharvested control and aggregate crown retention treatments but is reduced in dispersed treatments (Boyden et al., 2012) (Fig. 1).

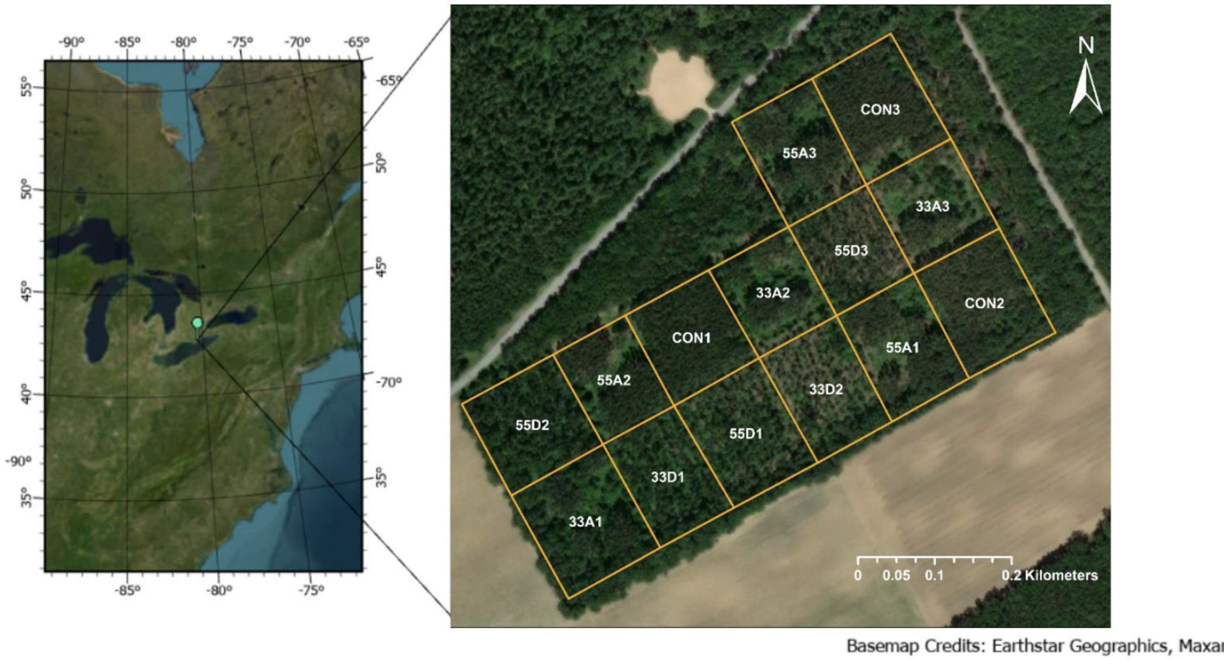


**Fig. 1.** Location of the red pine stand in Southern Ontario, Canada (left). An aerial view of the study site, divided into 14 1-ha plots (right). The three-digit abbreviation of each plot represents the variable retention harvesting treatment applied (see Table 1), and the last number is the replication number.

**Table 1.** Characteristics of the variable retention harvesting (VRH) treatments in the red pine stand. The canopy is primarily composed of red pine (*Pinus resinosa*), accompanied with a few other tree species, including white pine (*Pinus strobus*) and black oak (*Quercus velutina*). According to a pre-harvest survey in 2011, the mean height of red pine was 23.8 ± 2.8m (Zugic et al., 2021). The mean diameter at breast height and age of trees in the study site are 28.3 cm and 93 years old respectively (Bodo & Arain, 2022). The stand density represents the average density post-VRH treatment (So et al., 2024).

| Plot Abbreviation | Basal area retained post-VRH treatment (%) | Pattern of thinning | Stand Density (trees $plot^{-1}$) |
|---|---|---|---|
| CON | 100 | No thinning | 432 |
| 33A | 33 | Aggregate | 178 |
| 33D | 33 | Dispersed | 118 |
| 55A | 55 | Aggregate | 213 |
| 55D | 55 | Dispersed | 235 |

*1.2.2 Data*

We collected LiDAR data and RGB imagery of the study site in July of 2023 using a DJI Matrice 600 remotely piloted UAV fitted with an integrated Riegel MiniVUX-1 LiDAR sensor. The UAV was flown at 60m above ground level and LiDAR data was acquired with scan lines separated by 0.1m and constrained to a 120° field of view. The flight plan used parallel flight lines spaced 22m apart, resulting in images with 75% sidelap and 80% forward overlap, and a ground sampling distance of 0.01-0.02 m. After processing, the LiDAR data yielded an average point density of 650.7 points/$m^2$. LiDAR data covered all 14 plots of the study site, but RGB imagery in the northern corner and eastern section of the site, including plots 55A2, 55D2, and 33A1, were constrained by orthorectification limitations and were excluded.

We also collected tree height, crown diameter, and DBH field measurements for 72 trees in the study site. Only 57 of these trees were within the extent of the RGB imagery coverage. Height was calculated from the average measurements taken by a clinometer and a Nikon Forestry Pro II Laser Rangefinder. Crown diameter was derived from the average crown measurements in the north-south and east-west directions. DBH was collected using measuring tape at 1.3m above the ground. We also recorded the geographic locations of the sampled trees using GPS. To capture the leaf-off season, LiDAR, RGB, and field data were also collected in December of 2023 using the same sampled trees.

### *1.2.3 Individual Tree Detection and Delineation*

We constructed a 0.25m resolution CHM from the LiDAR point cloud and identified tree locations and heights using a local maximum filter with a window size of 2 meters. We applied a height threshold between 15-40m to obtain mature trees and delineated crowns using an MCWS algorithm. The treetops are inverted into sinks and stratified into several layers based on height interval. A pouring algorithm fills starting from the lowest layers with water until the sink is completely filled (Yun et al., 2021). Tree crowns are delineated using the edge of the water in each pit, yielding crown area, which is used to calculate crown diameter with the assumption that the crown is circular to address hidden coverage due to overlapping (Equation 1):

$$CD = 2\sqrt{\frac{CA}{\pi}} \qquad (1)$$

where *CD* is crown diameter and *CA* is crown area.

Local maximum filter and MCWS were applied for both leaf-on and leaf-off CHM. Tree crowns were classified into hardwood or softwood species using a ΔCA threshold calculated from leaf-on and leaf-off CHMs. This threshold was derived from a previous survey of seasonal canopy variation in the study site and differed between VRH treatments (So et al., 2024).

To generate self-supervised predictions from RGB imagery, we used an open-source deep learning neural network developed by Weinstein et al. (2019). The convolutional neural network uses a RetinaNet one-stage detector, which combines object detection and classification into a single network for faster training and decreased sensitivity to the magnitude of bounding box proposals. For classification, the neural network uses a ResBet-50 backbone pre-trained on an ImageNet dataset. The original neural network was trained on data from the National Ecological Observatory Network, but we trained the model using the delineated crowns derived from the MCWS algorithm (Weinstein et al., 2020). We divided the RGB images and the predictions from MCWS into spatial subsets for each individual plot in the study site to minimize overfitting between thinning treatments. The RGB images have a spatial resolution of 0.05m and were split into window sizes of 400 by 400 pixels to provide adequate context for tree detection. To account for the high stand density of the study site, we allowed a window overlap of 25% to capture trees divided among images (Weinstein et al., 2019). For each spatial subset of LiDAR-derived crown polygons, we extracted bounding boxes and used them as annotations for training. Bounding box predictions generated from the model were merged with height and crown perimeter information of polygons generated from the unsupervised LiDAR algorithm based on intersection over union threshold. We applied a weighted logarithmic algorithm based on the perimeter of the crown predictions to define crown diameter and shared boundaries between overlapping predictions (Hu & Jung, 2021; Wu et al., 2016) (Fig. 2).

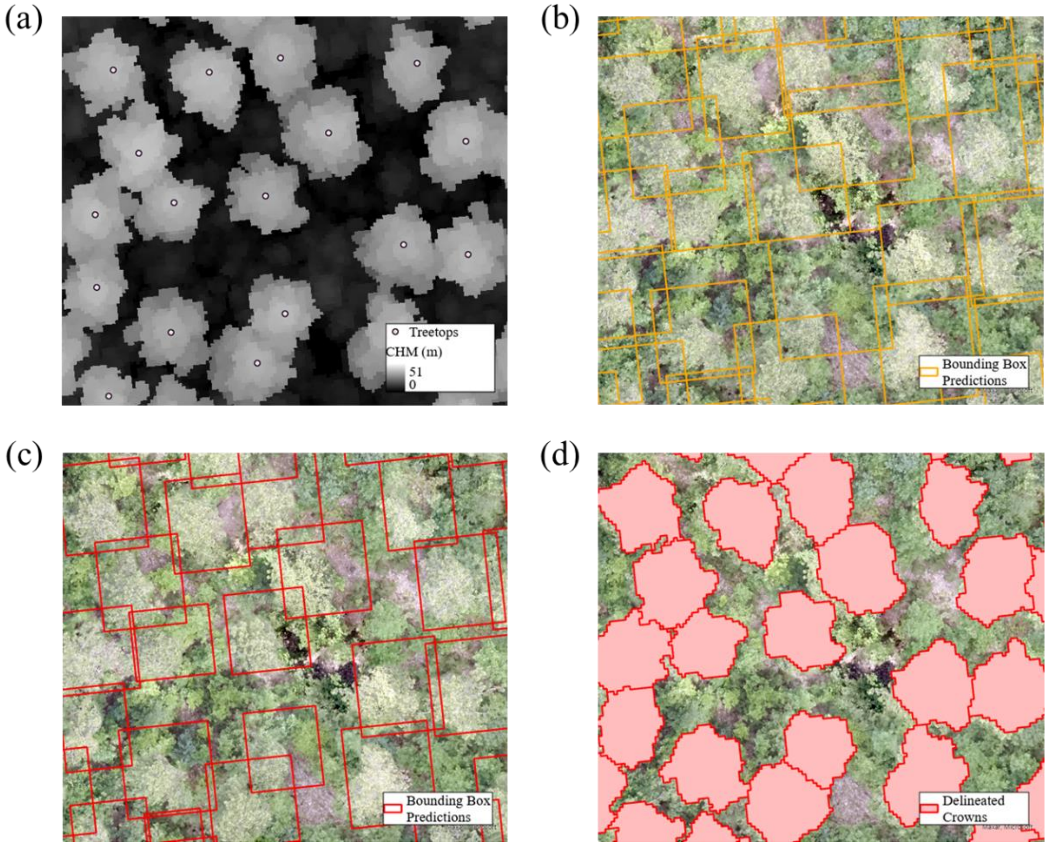


**Fig. 2.** Workflow for generating self-supervised red, green, and blue (RGB) delineated crowns. (a) Treetop detection using local maximum filtering and canopy height model from light detection and ranging point cloud, (b) bounding box annotations of crowns delineated by marker-controlled watershed segmentation for training, (c) bounding box predictions by self-supervised RGB deep learning model, and (d) delineated crowns of self-supervised RGB bounding box predictions using intersection over union threshold and weighted logarithmic algorithm.

*1.2.4 Tree-level Aboveground Biomass Estimation and Validation*

The database Tallo contains nearly 500,000 records of field measurements from over 5000 tree species worldwide. We identified 22 common tree species in Canada and extracted DBH, crown diameter, and biomass information for the species records, both in open and closed-canopy forests (Jucker et al., 2022). We conducted a regression analysis between DBH and crown diameter to create crown diameter-based AGB allometric equations for each species found in our study site (Table 2) (Gering & May, 1995; Hemery et al., 2005).

**Table 2.** Parameters derived for allometric equations were used to predict the diameter at breast height (DBH, cm) from crown diameter (m) for common tree species found at the study site. The relationship between DBH and crown diameter was significant for all species. The parameters *a* and *b* are exponents of the weight function of the equations provided by Lambert et al. (2005). The values for the parameters were derived from regression analysis of archival DBH, crown diameter, and biomass data collected by Jucker et al. (2022). *n* represents the number of data records used for each species.

| **Species** | ***a*** | ***b*** | **p-value** | $R_a^2$ | **n** |
|---|---|---|---|---|---|
| Red Maple | 2.806992458 | 3.504022233 | $< 2.2 \cdot 10^{-16}$ | 0.438960047 | 745 |
| Sugar Maple | 3.911188043 | -0.532628866 | $< 2.2 \cdot 10^{-16}$ | 0.572270107 | 4840 |
| Eastern White Pine | 5.173398317 | 1.024282383 | $< 2.2 \cdot 10^{-16}$ | 0.660361561 | 328 |
| Red Oak | 3.640308391 | 3.613734121 | $< 2.2 \cdot 10^{-16}$ | 0.676487076 | 477 |
| Black Cherry | 4.280098995 | -0.46564346 | $8.761 \cdot 10^{-15}$ | 0.529246468 | 79 |
| Red Pine | 5.497935919 | 4.336751745 | $< 2.2 \cdot 10^{-16}$ | 0.669898369 | 78 |
| Black Oak | 3.544180093 | 4.120237777 | $< 2.2 \cdot 10^{-16}$ | 0.683712703 | 105 |

The crown diameter-based equations were substituted into existing DBH-based allometric equations provided by Lambert et al. (2005) (Equation 2). The parameters $a$ and $b$ are exponents of the weight function of these allometric equations. Species specific parameter values were derived from archival DBH, crown diameter, and biomass data collected by Jucker et al. (2022):

$$DBH = a \cdot CD + b \qquad (2)$$

The DBH is then used to calculate AGB from estimated model parameters for each species' respective biomass component ($\beta_i$) (Equations 3, 4):

$$AGB_{total} = AGB_{wood} + AGB_{bark} + AGB_{foliage} + AGB_{branches} \qquad (3)$$

$$AGB_i = \beta_{i1} \cdot DBH^{\beta i2} \cdot H^{\beta i3} \qquad (4)$$

where $H$ is the tree height.

We also estimated the AGB change (ΔAGB) of trees using the delineated crowns and previous DBH inventory data before application of VRH treatments from the study site. We extracted DBH from the crown diameter of delineated crowns using Equation 2 and calculated ΔAGB using a survey of mean annual DBH change of mature trees in the site after VRH treatment was implemented.

Delineated crowns generated from the unsupervised and self-supervised predictions were matched with ground validation data through a direct intersection between the crown polygon and the ground truth location. We assessed the detection rate as the proportion of ground truth trees matched with the predicted crowns. AGB in the ground validation data was calculated from height and DBH measurements using Equations 3 and 4. We used adjusted $R^2$ ($R_a^2$) and root mean squared error (*RMSE*) as accuracy metrics to evaluate the performance of the crown diameter, tree height, and AGB predictions with the ground validation data.

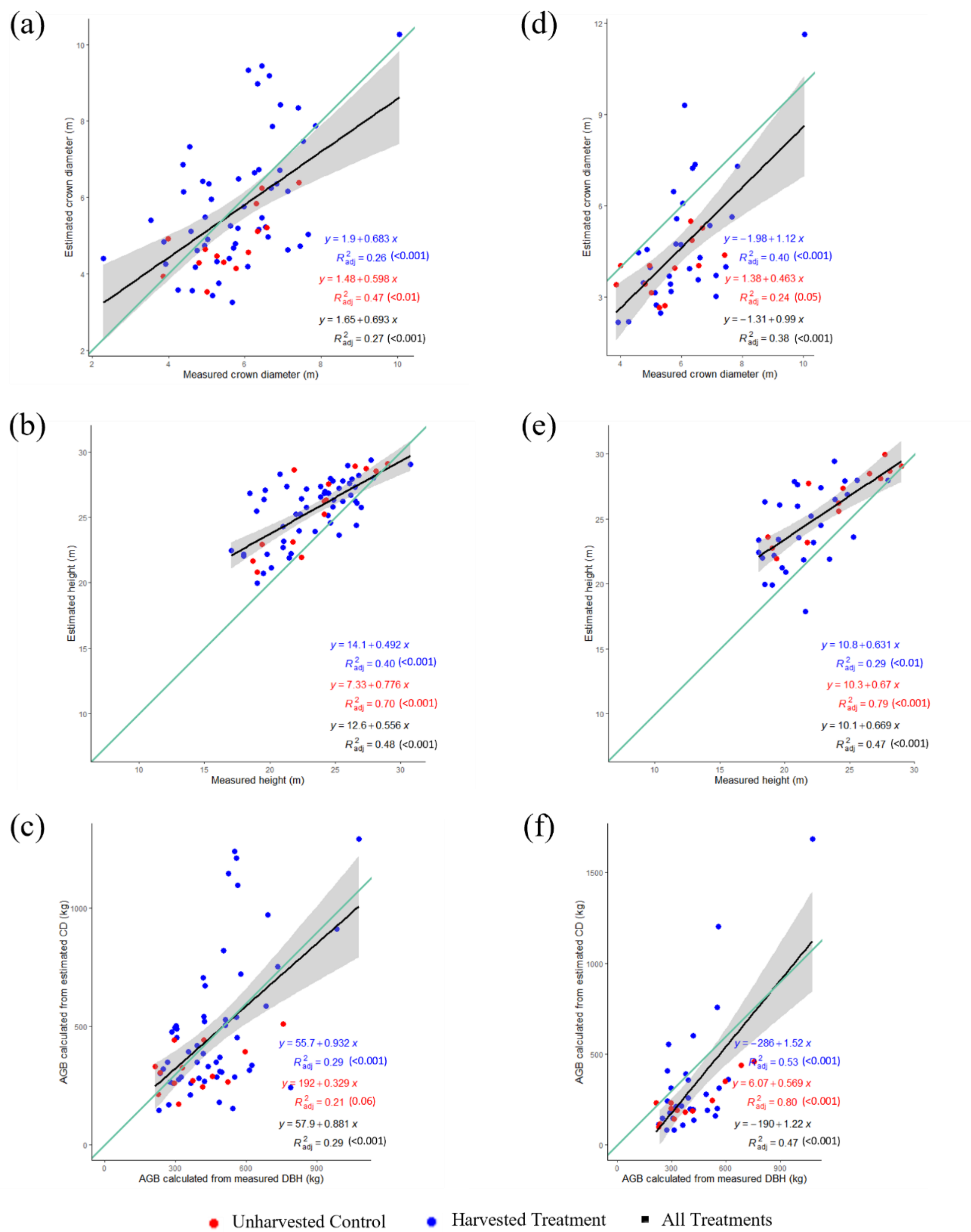


**Fig. 3.** Comparisons of the estimated (a) crown diameter, (b) height, and (c) aboveground biomass (AGB) calculated using allometric equations developed from unsupervised light detection and ranging data against ground measurements. $n$ = *67*. Comparisons are also provided for the

estimated (d) crown diameter, (e) height, and (f) AGB calculated using allometric equations developed from self-supervised red, green, and blue deep learning predictions against ground measurements. $n = 43$. The equations for the line of best fit and the adjusted $R^2$ ($R_a^2$) values for the unharvested control and for all variable retention harvesting treatments are displayed. The p values for the $R_a^2$ are displayed in parentheses. The black line indicates the regression fit line while grey shade shows the 95% confidence intervals of mean prediction for the regression line. The green line is the 1:1 line.

### *1.3 Results*

We first analysed the performance of crown delineation, height and AGB estimations from UAV LiDAR data. Initial treetop detection and crown delineation using the unsupervised LiDAR-based algorithm identified 5122 trees in the study site with average and range height of 24.4m and 15.0m – 34.0m, respectively. Stand height is consistent with a pre-harvest forest inventory survey of the site conducted in 2011, which yielded a mean height of 23.8 ± 2.8m (Zugic et al., 2021). The estimated mean and range of the crown diameter were 5.0m and 1.2m – 15.4m, respectively. Crowns delineated with the unsupervised LiDAR algorithm matched 67 trees in the ground truth data, with a detection rate of 93.06%. Overall, estimations for height ($R_a^2$= 0.48, p= <0.001, RMSE= 3.15m) were stronger than crown diameter ($R_a^2$= 0.27, p= <0.001, RMSE= 1.42m) (Fig. 3). Amongst the treatments, model performances for crown diameter ($R_a^2$= 0.47, p= <0.01) and height ($R_a^2$= 0.70, p= <0.001) estimations were strongest in the unharvested control plot. AGB estimations in the harvested treatment plots (mean across harvested treatments $R_a^2$= 0.29, mean p= <0.001) outperformed the unharvested control plots ($R_a^2$= 0.21, p= 0.06) (Fig. 3 (c)).

Treetop detection and crown delineation using the self-supervised RGB model identified 3482 trees within the spatial extent of the RGB imagery. The trees have a height and crown diameter mean of 24.01m and 4.95m, respectively. Crowns delineated with the self-supervised RGB model matched 43 trees in the ground truth data, with a detection rate of 75.44%. Overall, RGB-based predictions for crown diameter ($R_a^2$= 0.38, p= <0.001, RMSE= 1.99m) and AGB ($R_a^2$= 0.47, p= <0.001, RMSE= 236.58 kg) outperformed their respective LiDAR-based predictions (Crown diameter $R_a^2$= 0.27, Crown diameter p= <0.001, Crown diameter RMSE= 1.42m, AGB $R_a^2$= 0.29, AGB p= <0.001, AGB RMSE= 229.35 kg) while height predictions remained even (LiDAR $R_a^2$= 0.48, LiDAR p= <0.001, LiDAR RMSE= 3.15m, RGB $R_a^2$= 0.47, RGB p= <0.001, RGB RMSE= 3.57m) (Fig. 3). Amongst the treatments, predictions for height ($R_a^2$= 0.79, p= <0.001) and estimated AGB ($R_a^2$= 0.80, p= <0.001) were strongest in the unharvested control (Fig. 3(e)& 3(f)). However, crown diameter predictions in the unharvested control plot were weaker than in the harvested treatment plots (Control $R_a^2$= 0.24, Control p= 0.05, mean across harvested treatments $R_a^2$= 0.40, mean p= <0.001), and performed worse than fully-supervised deep learning approaches (Brandt et al., 2020) (Fig. 3(d)).

**Table 3.** Summary statistics for the performance of the estimated aboveground biomass (AGB) based on tree height and crown diameter derived from unsupervised light detection and ranging data and self-supervised red, green and blue deep learning model. AGB adjusted $R^2$ ($R_a^2$) is provided for each control (unharvested) and variable retention harvesting (VRH) treatments that were applied for the study site and include average stand density and basal area retained post-VRH treatment (So et al., 2024). The p values for the $R_a^2$ are displayed in parentheses.

| **Thinning Treatment** | **Basal Area Retained (%)** | **Stand Density (trees plot$^{-1}$)** | **$R_a^2$ LiDAR ($n = 67$)** | **$R_a^2$ RGB ($n = 43$)** |
|---|---|---|---|---|
| Control | 100 | 432 | 0.21 (0.06) | 0.80 (<0.001) |
| Aggregated | 33 | 178 | 0.40 (<0.01) | 0.79 (<0.001) |
| Aggregated | 55 | 213 | 0.04 (0.24) | 0.34 (0.13) |
| Dispersed | 33 | 118 | 0.39 (0.11) | 0.66 (<0.05) |
| Dispersed | 55 | 235 | 0.31 (<0.05) | 0.19 (0.18) |
| **Overall** | | 223 | 0.29 (<0.001) | 0.47 (<0.001) |

Amongst harvested treatments, AGB estimation from both LiDAR and RGB data is most accurate when 33% of the basal area is retained (mean across LiDAR 33A and 33D $R_a^2$= 0.40, mean across LiDAR 33A and 33D p= <0.05, mean across RGB 33A and 33D $R_a^2$= 0.73, mean across RGB 33A and 33D p= <0.001), which are also the treatments with the lowest stand density. Dispersed treatments with reduced tree clumping perform worse with self-supervised RGB deep learning than aggregate treatments (mean across 33D and 55D $R_a^2$= 0.43, mean across 33D and 55D p= <0.05, mean across 33A and 55A $R_a^2$= 0.57, mean across 33A and 55A p= <0.001). For unsupervised LiDAR predictions, aggregate treatments that retain baseline tree clumping performed evenly with dispersed treatments when treatment is severe (33A $R_a^2$= 0.40, 33A p= <0.01, 33D $R_a^2$= 0.39, 33D p= 0.11), but much weaker in moderate treatments (55A $R_a^2$= 0.04, 55A p= 0.24, 55D $R_a^2$= 0.31, 55D p= <0.05) (Table 3) (Boyden et al., 2012; So et al., 2024).

Amongst the delineated crowns generated by the self-supervised RGB model, the total estimated AGB of mature trees in the study site is 1006042 kg, with a density of 10.1 kg $m^{-2}$ across the spatial extent of the RGB imagery. AGB density in the unharvested control (16.5 kg $m^{-2}$) is consistent with estimates for other unharvested forest stands within the same ecoregion (Barakat, 2017). Amongst harvested treatments, the AGB density is higher with moderate VRH (mean across 55A and 55D= 9.3 kg $m^{-2}$, mean p= <0.001) compared to severe VRH (mean across 33A and 33D= 7.1 kg $m^{-2}$, mean p= <0.001), and comparable between aggregate thinning (mean across 33A and 55A= 8.4 kg $m^{-2}$, mean p= <0.001), and dispersed thinning (mean across 33D and 55D= 8.0 kg $m^{-2}$, mean p= <0.001) (Fig. 4(a)). The mean annual ΔAGB density for the study area is 0.15 kg $yr^{-1}$ $m^{-2}$, with the mean annual ΔAGB density greater in the unharvested control plots (mean= 0.18 kg $yr^{-1}$ $m^{-2}$) compared to the harvested treatment plots (mean across harvested treatments= 0.15 kg $yr^{-1}$ $m^{-2}$, mean p= <0.001). In harvested treatments, annual ΔAGB density is lower in moderate VRH (mean across 55A and 55D= 0.09 kg $yr^{-1}$ $m^{-2}$, mean p= <0.001) compared to severe VRH (mean across 33A and 33D= 0.21 kg $yr^{-1}$ $m^{-2}$, mean p= <0.001), while annual ΔAGB density is higher in dispersed thinning (mean across 33D and 55D= 0.17 kg $yr^{-1}$ $m^{-2}$, mean p= <0.001) compared to aggregate thinning (mean across 33A and 55A= 0.13 kg $yr^{-1}$ $m^{-2}$, mean p= <0.001) (Fig. 4(b)).

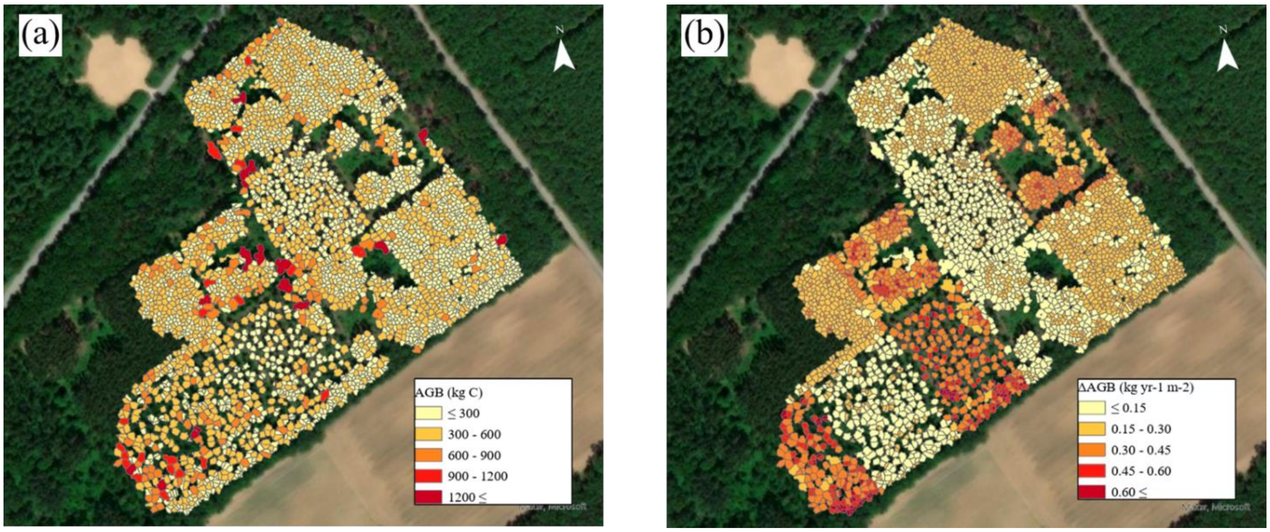


**Fig. 4.** Comparisons of the estimated (a) aboveground biomass (AGB) and (b) the annual AGB change density calculated using allometric equations developed from self-supervised red, green, and blue deep learning predictions against ground measurements.

### *1.4 Discussion and summary*

#### *1.4.1 LiDAR and RGB-based Tree Height Estimation and Crown Delineation*

In this study, we demonstrated the feasibility of using UAV LiDAR and RGB data for estimating tree-level canopy height, crown area and eventually AGB for a 14 1-ha forest stands with various stand density and tree distribution. Our approach combines an unsupervised LiDAR segmentation algorithm and a self-supervised RGB deep learning model to improve forest inventory data collection, particularly under VRH treatments. The unsupervised LiDAR method applied a modified MCWS for tree crown delineation, while tree heights were extracted using a local-maxima filtering approach. A self-supervised deep learning model was trained on RGB imagery using LiDAR-derived annotations, allowing crown delineation in the absence of extensive ground truth data. This dual approach aimed to assess AGB estimation accuracy across different forest stand structures and management regimes. When comparing with UAV LiDAR-based studies conducted in unharvested forests in other regions across the world, the performance of our unsupervised LiDAR algorithm is consistent with local maximum filtering for height, but weaker with inverse watershed segmentation of tree crowns. Panagiotidis et al. (2016) yielded a similar height accuracy ($R_a^2$= 0.72 – 0.75) and stronger crown delineation ($R_a^2$= 0.63 – 0.85) in a smaller, primarily coniferous forest.

There are three major challenges with delineating tree crowns using LiDAR, which are reflected in the unsupervised LiDAR algorithm. First, treetop detection is limited in mixed forests, with omission errors common for smaller crown structures and trees hidden under the canopy (Yun et al., 2021). Leaf-off LiDAR aided in the detection and classification of smaller hardwood trees within the study area, but improvement is marginal when mixed with taller softwood trees. Canopy compositions in stands undergoing VRH treatments are less dominated by mature red pine trees, and the improved pulse penetration enables more accurate capture of inventory data (Gatziolis et al., 2010; So et al., 2024). Second, the water pouring algorithm in MCWS relies on height variation for region expansion, particularly along crown boundaries, to avoid over-expansion. Height variation is greater in plots with lower stand densities or undergoing dispersed VRH treatment where mature red pines are more spread apart, improving differentiation between water expansion boundary cells and adjacent treetops (Lisiewicz, 2022). Our approach applies two solutions, using high resolution LiDAR point cloud to construct the CHM to help preserve some height variation and masking non-tree areas with a height threshold to allow clearer segmentation along boundaries (Yin & Wang, 2019). Third, tree clumping is particularly prevalent in mixed and deciduous forest stands, with commission error in treetop detection common with regenerating broadleaf trees. Young broadleaf stands such as black oak or red maple (*Acer rubrum*) fill the harvested gaps left behind by aggregate VRH, and false positives may occur when delineating large canopies due to multi-foliage clumps and lateral branches. We screen out over-segmentation using an angle threshold between height and spatial distance differences, improving delineation in dispersed and unharvested treatments where broadleaf and coniferous species are more evenly mixed (Hu et al., 2014; Yun et al., 2021).

These challenges with LiDAR-based tree crown delineation highlight the mixed performances of AGB estimations, especially when applied with our crown diameter-based allometric equations. Training the self-supervised RGB model on LiDAR-derived annotations addresses the lack of training data available for forests undergoing VRH treatment. Incorporating the vertical and colour features of trees into the deep learning approach limited the under and over-segmentation of crowns observed with unsupervised LiDAR delineation. The self-supervised RGB model is less effective when delineating crowns in more complex canopy conditions such as the unharvested control, and existing models that are pretrained on much larger datasets would be better suited for unmanaged forests. A more complex convolutional neural network that refines bounding box classification using additional features like shadows may aid with crown boundary identification (Qi, 2017). In previous studies, crown size has been used to develop regression models for tree height in Canadian forests, particularly in stands with uniform species or age. The crown-height relationship is less clear in mixed forests with complex horizontal and vertical structures, and accurate crown-to-height prediction using RGB-based deep learning delineations would require additional species and age labeling from manual annotations (Falkowski et al., 2014; Russell et al., 2014). For height estimation, crown delineations generated by self-supervised RGB model are more effective for developing a crown boundary mask to extract tree height from the CHM.

### *1.4.2 Tree-level AGB Estimation*

Quantifying AGB in stands depends on accurate relationships between key biomass determinants such as height and crown area. Although growth models often project an inverse relationship between height and crown diameter, MCWS may inaccurately capture crown ratio as the full crown of taller trees are segmented and the canopies of smaller trees are partially hidden. The variance in height and crown between in-situ measurements and LiDAR methods leads to disagreements in AGB estimates (Garber et al., 2008). Inaccurate AGB estimations also occur due to overestimation of tree height in stands of varying tree apex and branch structures. Integrating height into the weighted analysis of initial crown delineations from the RGB deep learning model helps account for age, structure, and species-specific changes in crown ratio. Although this approach can lead to crown underestimation in taller trees, incorporating crown recession in AGB estimates reflects in-situ observations better than unsupervised algorithms relying solely on airborne laser scanning (Van Deusen & Heath, 2010). Nevertheless, both unsupervised LiDAR and self-supervised RGB approaches are less impacted by canopy obstruction and tree apex variance in stands with smaller densities. Especially in severely managed forests, a smaller density of residual trees allows accurate capture of vertical structure and full canopy profile, resulting in more precise sinks for MCWS and subsequently higher quality annotations for deep learning model training.

Trees in stands undergoing moderate dispersed harvesting are spaced closer together compared to severe dispersed treatment stands, which can make tree classification for species-specific allometric AGB equations more difficult. It is less of an issue for unsupervised LiDAR predictions, where mature softwood and young hardwood trees can be differentiated by height threshold and crown area change between leaf-on and leaf-off seasons. However, species classification using spectral signatures is unreliable in crowded mixed stands of softwood and hardwood trees. Species common in mixed coniferous and deciduous forests have similar spectral reflectance properties in the visible spectrum, which may lead to species misclassification in AGB estimation. A self-supervised deep learning model relying on imagery would need to use near-infrared reflectance or additional properties such as texture or seasonal phenology (Martin et al., 1998). In moderate aggregate treatment, hardwoods and softwoods are clumped separately into dense homogenous groups, allowing the self-supervised deep learning model to pick up on minor differences in spectral signatures between species more easily. In contrast, dense clusters of trees with similar height and crown structure can lead to high overlap between branches and crown boundaries, leading to missed or under-segmented crowns (Wan Mohd Jaafar et al., 2018).

The allometric equations used to estimate DBH from height and crown diameter leave room for improvement. While Equation 1 standardizes irregular canopies and aids with automation, AGB estimation requires a more comprehensive approach to geometric differences in crown area (Kutchartt et al., 2024). Our allometric equations account for interspecies variation in the crown diameter-to-area relationship but could not also consider VRH treatments due to the lack of available archival DBH, crown diameter, and biomass data for VRH sites in Canada.

### *1.4.3 Biomass Growth Response of VRH*

The study area is located within the Carolinian zone of southern Ontario, an ecoregion characterized by high biodiversity and vegetation growth (Barakat, 2017). The rich growth environment enhances biomass regeneration, especially in comparison to other mixed forests undergoing active harvest management (Boucher et al., 2021; Molina et al., 2021). Canopy gaps left behind in harvest treatment plots enhance below-canopy light environment and encourage advanced regeneration of red pine and other species (Nyamai et al., 2020). However, most broadleaf stands in our site were within the understory layer and too short to be fully delineated by the self-supervised RGB deep learning model which is trained on mature crowns. Softwood species also contain less biomass across all tree components compared to residual red pines, which contribute the most to mature tree AGB as reflected in biomass trends between stand densities (Westfall, 2012). Nonetheless, tree biomass growth benefits from gaps within the forest matrix created by VRH treatments, which limits competition for sunlight and nutrients with neighbouring trees. Particularly at higher intensities, thinning treatments like VRH reduce horizontal-spacing competition amongst mature trees, enhancing biomass growth through increased access to resources (Kim et al., 2015). The effect is limited in aggregate thinning, where horizontal-spacing between trees is minimally changed and excessive clustered gaps within the forest matrix introduce soil drainage problems (Kanninen et al., 2004). Overall, amongst VRH treatments in our study, biomass growth benefits the most from severe dispersed thinning and the least from moderate aggregate thinning, consistent with previous in-situ studies conducted in our site (e.g., Zugic et al. (2021)).

### *1.4.4 Conclusions and Outlook*

While our self-supervised deep learning approach can be reproducible in small forests with local LiDAR and RGB datasets, there are two major limitations when extrapolating height and crown information to other biophysical characteristics. First, allometric DBH and AGB relationships were derived from a database that may be incompatible with certain biomass models. Specifically, biomass components such as foliage or fruit are unavailable, and some trees were excluded due to the lack of crown diameter data. Data availability for common Canadian tree species is also limited, so we grouped some missing species into general softwood or hardwood categories for DBH and AGB calculations (He et al., 2013; Jucker et al., 2022). We recommend exploring local datasets to supplement the estimation of stand inventory in mixed forests as the relationship between height and crown diameter, and eventually with AGB can vary between forest management, growth environment, species composition, and other factors. A more recent forest inventory database that includes isolated forests with natural ecosystems and different stand densities can expand the scope and application of our allometric equations. Second, while delineated crowns from a self-supervised RGB model provide an automated and substantially cheaper alternative to quantifying AGB and ΔAGB, it does not take into consideration shrubs and young trees in its estimation, only the sizeable trees. The height thresholds required for proper delineation of crown boundaries mask understory vegetation and short trees, and the approach might work best for assessing biomass and C uptake changes in forests where the understory is a small contributor (Bodo et al., 2023). Thus, estimates made by the self-supervised method should be considered as additional reference data in guiding forest management pathways rather than a primary indicator for long-term trends in biomass growth and climate mitigation at all levels of an ecosystem. We suggest additional research into self-supervised crown delineation and height estimation in stands dominated by broadleaf species or young saplings.

Although our study was limited to 3482 – 5122 trees across a 14-ha plot, it provides insight into integrating multi-source remote sensing data and self-supervised algorithms into forest inventory programs on a large scale to improve the efficiency of acquiring information critical to the sustainable management of forests for climate change. Nonetheless, our study is complemented by varying shape and intensity of experimental thinning which was expected to have the largest impact on crown and tree dimension relationship with AGB to construct allometric equations. MCWS, when supplemented with self-supervised deep learning, was particularly effective in estimating biomass components in unharvested and severely thinned forests. This approach is a cheaper and less labour-intensive forest inventory alternative to traditional in-situ methods, only dependent on availability of aerial LiDAR data and RGB imagery. It can be useful for tracking biomass and forest C storages changes across time and management regions, such as plantations before and after a harvest treatment. To expand on the applications of self-supervised deep learning from remote sensing observations, our approach should be tested to evaluate biomass outcomes of other silvicultural interventions and forest management. We also encourage further research on the application of unsupervised LiDAR-based crown delineations for training other neural network architectures, such as U-Net, that can operate on limited amounts of annotations. As deep learning neural networks are becoming more popular as a method for tree crown delineation and biomass estimation, the accuracy and performance of the predictions must be properly evaluated, particularly in the context of mixed forest stands with complex canopy structures and biodiversity.

# Chapter 2: Impacts of Retention Harvesting on Species Biodiversity and Richness

## *2.1 Introduction*

We have extensively covered VRH treatments in the context of stand regeneration and biomass growth rate. However, another critical objective of VRH is to benefit biodiversity through the retention of key forest structures (e.g. live and dead trees, wood debris) in production stands (Gustafsson et al., 2020). Microenvironmental changes brought forth by selective harvesting can affect the formation of understory vegetation, improving species diversity and resilience to climate change impacts (Deng et al., 2023). Studies have shown VRH enhances stand-level structural characteristics, subsequently creating favourable conditions for understory biodiversity conservation. For instance, in wildfire-prone forests, dispersed retention treatments have been associated with increased understory vegetation cover and species richness compared to unharvested controls (Franklin et al., 2019). Similarly, Franklin et al. (2018) found that combined aggregated and dispersed retention was also effective in supporting species diversity in understory communities within boreal mixedwood forests. VRH was implemented in our red pine plantation stand in 2014 for a similar objective: to modify the structural complexity of the canopy and enhance the biodiversity of plant species. In a previous study of the area, we found that aggregate and dispersed treatments generally create favourable microclimate conditions for the understory. Unlike clearcut or unharvested forest stands, VRH increases the light environment to encourage understory C uptake, while simultaneously retaining enough trees to provide a litter-rich environment (So et al., 2024).

However, red pines are known to be allelopathic, and forests are typically characterized by sparse understory vegetation even with favourable light conditions. The needle-like litter of red pines are rich in resin acids, which degrade into active growth inhibitory substances for several broadleaf and herbaceous species. For example, sufficient concentrations of 15-hydroxy-7-oxodehydroabietate and 7-oxodehydroabietic acid, formed from the degradation of Japanese red pine (*Pinus densiflora*) resin, can inhibit the growth of invasive grass and weed species (Kato-Noguchi et al., 2017). Thus, even with enhanced forest management practices providing greater access to sunlight, nutrients, and water in the understory, the allelopathic effects of red pine litter can persistently inhibit the growth of non-pine species (Spitale, 2011). There is a possibility that biochemical responses of VRH observed in our study area reflect a homogenized understory dominated by pine saplings. The dominance of red pine in the overstory and its associated allelopathic suppression of woody and herbaceous species can encourage a feedback loop, where only red pine saplings can establish and thrive, further reinforcing the monoculture through the defoliation and degradation processes (So et al., 2024). Although the biodiversity benefits of VRH have been extensively documented for deciduous and coniferous mixedwood forests, the impact on species richness in single-layered monocultures with substantial allelopathic potential remains poorly understood. Therefore, despite the increased biomass regeneration and climate mitigation associated with VRH treatments in plantation stands, it is critical to understand their effects on the presence and abundance of native species to avoid establishing biological deserts with poor biodiversity (Spitale, 2011).

Furthermore, our study area is located over a dried stream bed, with predominantly sandy soil and wet conditions (So et al., 2024). Dried stream beds, remnants of intermittent fluvial systems, often exhibit heterogeneous microtopography and small-scale elevation gradients are common. Depressions may retain water longer while elevated areas may dry out more quickly, leading to a patchy distribution of soil nutrients across the landscape. This uneven elevation also creates microhabitats where water and solutes, including dissolved organic C and nitrate, can accumulate during precipitation events, leading to spatial variability in soil nutrient pools (Rupp et al., 2021). The leaching process of C and N is accelerated by periodical dry and wet conditions. During dry periods, organic matter decomposition slows, leading to the accumulation of soluble nutrients. Subsequent rewetting events can then mobilize these nutrients, resulting in pulses of leaching, a phenomenon known as the "Birch effect" (Zhu et al., 2022). Heterogeneity in soil nutrient stoichiometry due to elevation can lead to uneven vegetation patterns, limiting the establishment of certain species that require more nutrient-rich soil. Stand growth patterns in our study area suggest additional soil drainage issues caused by excessive removal of trees. But how these moisture and soil nutrient dynamics impact understory species richness has yet to be extensively studied in our site and other small-scale managed forests (So et al., 2024).

Here, we investigate the impacts of various VRH treatments on biodiversity and species presence in a red pine plantation stand in Canada. We plan to use a combination of digital hemispherical photography, remote sensing, and ground-based biometric measurements to assess light environment, litter input, soil nutrient content, topography, and understory species richness over a multi-VRH treatment mosaic. Through this work, we aim to demonstrate the impacts of differential retention strategies on microhabitat heterogeneity, nutrient cycling, and native species regeneration in red pine plantation ecosystems.

## *2.2 Materials and Methods*

### *2.2.1 Species Identification and Richness*

We carried out this study at the same temperate red pine plantation stand located within the St. Williams Conservation Reserve. The climate in this region is characterized by warm, humid summers and cold winters. The mean annual temperature is 8.0 °C and the mean annual precipitation is 1036 mm, of which approximately 13 % falls as snow (Arain et al., 2022). A pre-harvest survey of our study area identified 53 woody species in the understory, including vines, shrubs, and trees. Black cherry (*Prunus serotina*), black oak (*Quercus velutina*), red maple (*Acer rubrum*), and eastern white pine (*Pinus strobus*) primarily make up the woody understory layer, although several herbaceous species were noted in subsequent surveys (Bodo et al., 2023). Within each of the 14 1-ha plots, we established 5 georeferenced sampling points: 1 at the geographical center of the plot, and the other 4 at 20 m north, east, south, and west of the center (Fig. 5.). During the growing season in June of 2025, we collected high-resolution overhead photographs of a 1m by 1m quadrat plot at each sampling point. These photographs were captured at a height of 1.5m using a Nikon D750 camera equipped with an AF-S NIKKOR 14-24mm f/2.8G ED lens.

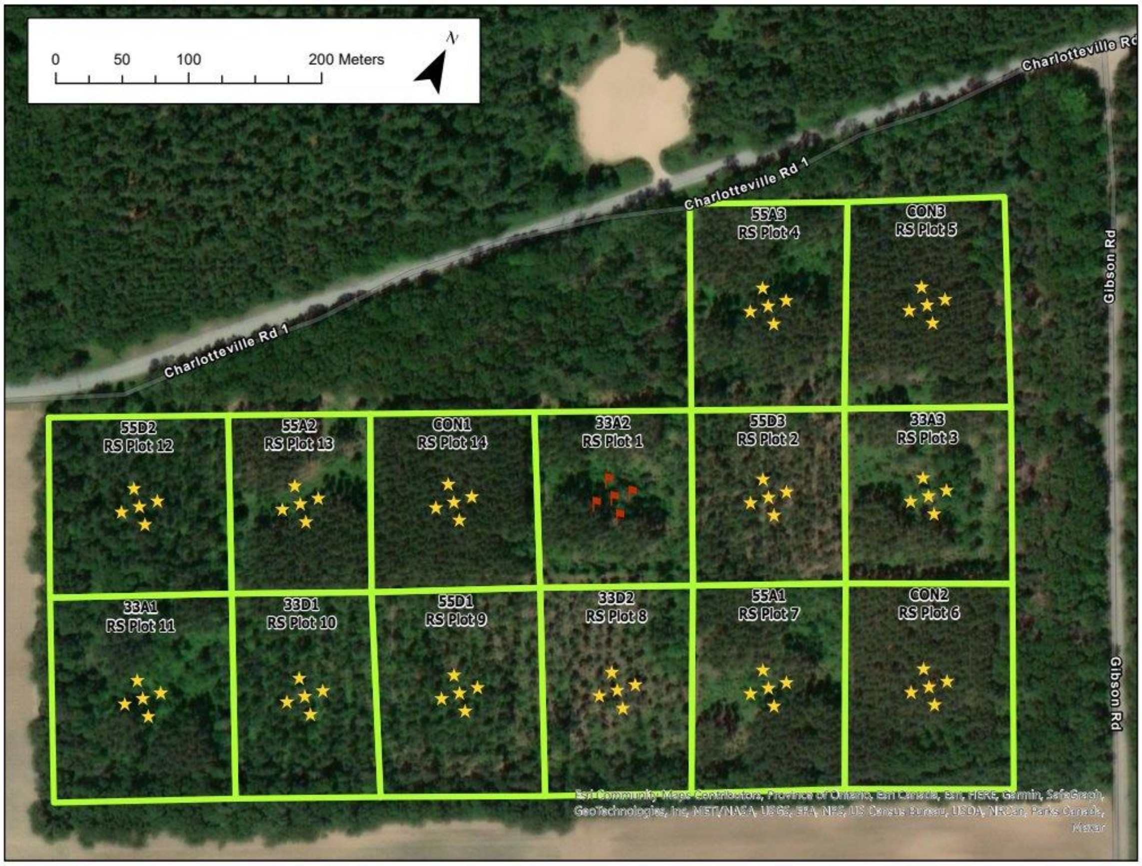


**Fig. 5.** Aerial view of the study site, divided into 14 1-ha plots. The three-digit abbreviation of each plot represents the variable retention harvesting (VRH) treatment applied, and the last number is the replication number. Within each plot, sampling points are established at the geographical center of the plot, and 20 m north, east, south, and west of the center, denoted by either a yellow star or red flag symbol.

We divided each quadrat plot photograph into 10cm by 10cm image tiles, filtered for green channel light using the image processing software ImageJ, and created a binary mask of black and white pixels separating the leaves from the background elements. To classify species, we used Leafsnap, a multi-stage computer vision system that first calculates leaf curvature using area and arclength measures. Disks of fixed radii are placed at each point along the leaf's contour to compute the fraction of area or perimeter lying within the segmented leaf, and then used to construct histograms of curvature over scale features. The features are used as queries for a nearest neighbours search of the Leafsnap database, which contains over 29000 images across 184 species, including primary woody species identified in our study area. Species are identified using curvature histogram intersection distance, a method that has previously yielded a 96.8% accuracy in returning the correct match for field images (Neeraj Kumar et al., 2012). For plants not covered in Leafsnap's database, like grasses and shrubs, we identified species using *Plants of Southern Ontario, Trees, Shrubs, Wildflowers, Grasses, Ferns and Aquatic Plants* by Richard Dickinson and France Royer, which contains 760 species of wild flora (Richard Dickinson & Royer, 2014).

To quantify species richness, we used the Chao1 estimator, which has a lower-bound estimate of true species richness. The index is based on the frequency of rare species observed, providing a more accurate estimate of richness in instances where rare species may be missed during sampling (Equation 5). This is particularly appropriate for our study area, given the within-site heterogeneity of habitat conditions, our limited sample size, and the stand's location in the highly biodiverse Carolinian Zone of southern Ontario (Chao et al., 2015):

$$S_1 = S_{obs} + \frac{(F1)^\wedge 2}{2 \cdot F2} \qquad (5)$$

where $S_1$ is the true species diversity, $S_{obs}$ is the number of species in the sample, $F_1$ is the number of singletons (species occurring only once in the sample), and $F_2$ is the number of doubletons (species occurring twice in the sample).

*2.2.2 Understory Radiation Measurements and Red Pine Canopy*

To quantify the concentration of photosynthetically active understory radiation, we measured the average daily photosynthetic photon flux density ($PPFD_U$) transmitted below the canopy (Jonckheere et al., 2005). At each sampling point, digital hemispherical photographs were taken on 12 dates throughout the 2022 growing season, using a Sigma 8 mm f/3.5 EX DG Circular Fisheye Lens. Through ImageJ, the photographs were filtered for blue channel light, and a binary mask of black and white pixels was created separating the sky and canopy elements. We used the CIMES program to extract the gap fraction, with the parameters set as 36 zenith rings, 144 azimuth sectors, and a zenith angle between 20° and 70°. The equation used by the program to calculate gap fraction is as follows (Gonsamo et al., 2011) (Equation 6):

$$P_0(\varphi,\theta) = P_W/(P_B + P_W) \qquad (6)$$

where $\varphi$ is the mid-point of the azimuth angle of a portion of the hemisphere projected to the image plane, $\theta$ is the mid-point of the zenith angle, $P_B$ is the number of canopy pixels, and $P_W$ is the number of sky pixels within the selected area of the image.

Results from the gap fraction analysis were used to estimate $PPFD_U$ through PARCLR.exe, an executable file from the CIMES program. We also used the program to calculate the leaf area index (LAI), a dimensionless variable to quantify red pine canopy foliage density based on one-half the total leaf area per unit of horizontal ground surface area (Gonsamo et al., 2011). The zenith angle was restricted to 50° -70° to prioritize red pine canopy close enough to the sampling point for litter to have an allelopathic effect on plant growth. We focused on photographs taken during early spring (March) and autumn (September), just before red pines drop their old needle-like leaves (Kato-Noguchi et al., 2017). LAI is calculated from null-gap segments using the executable files

LANG01.exe and LANG02.exe, using the following equations by Gonsamo et al. (2011) (Equations 7, 8):

$L_{SAT}(\theta,\varphi) = -2 \cdot \ln[1/N_{pixels}] \cdot \cos\theta$ (7)

$P_0(\theta,\varphi) = \exp[-L_{SAT}(\theta,\varphi) \cdot 0.5/\cos\theta]$ (8)

where $\theta$ is the zenith angle, $L_{SAT}(\theta,\varphi)$ is the maximum LAI value of a null-gap segment, $N_{pixels}$ is the number of pixels in the null-gap segment, and $P_0(\theta,\varphi)$ is the new null-gap segment.

### *2.2.3 Topography and Soil Nutrient Content Measurements*

We constructed a 1.0m resolution digital elevation model (DEM) of our study area from our LiDAR point cloud data (Fig. 6.). To predict water and nutrient pooling, we used the Topographic Wetness Index (TWI), which quantifies the spatial distribution of soil moisture based on local topography variation. TWI reflects the tendency of water to accumulate at a given location as a function of both slope and upstream contributing area. Data from the DEM was used to create a 1.0m TWI raster of the study site, calculated using the following equation (Beven & Kirkby, 1979) (Equation 9):

$\mathrm{TWI} = \ln\left(\frac{a}{\tan(\beta)}\right)$ (9)

where $a$ is the upslope contributing area to the flow direction and $\beta$ is the local slope angle.

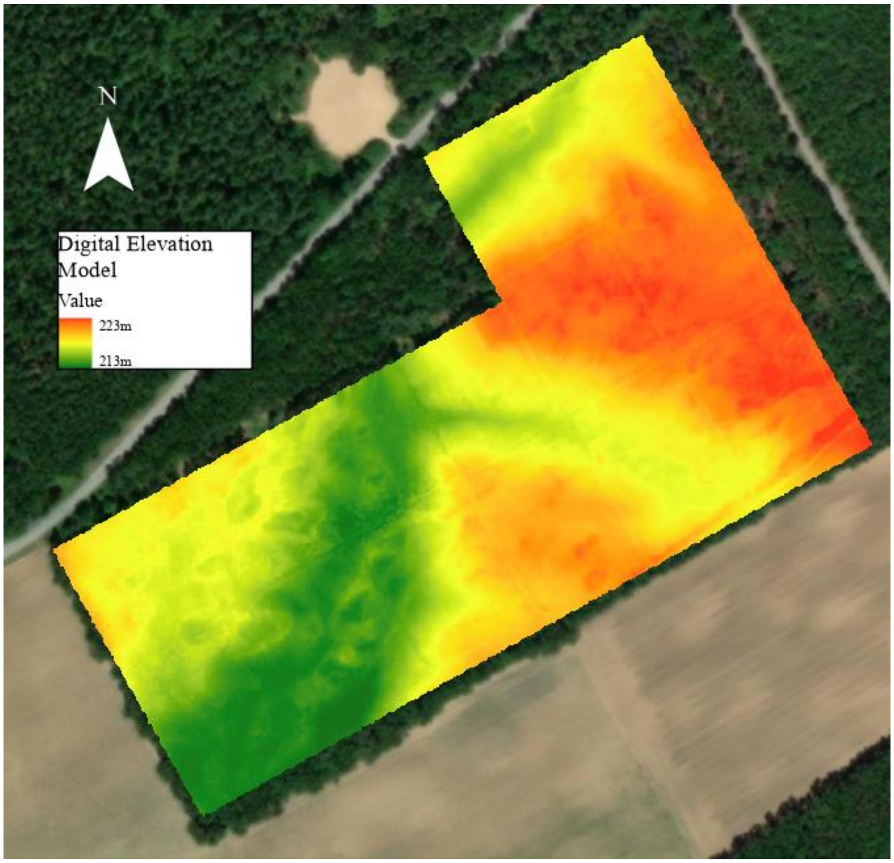


**Fig. 6.** Digital elevation model of the study site, at 1.0m resolution. The model was constructed from light detection and ranging point cloud data collected in July of 2023.

We also collected soil core samples to a depth of 10 cm at 4 sampling points located 20 m north, east, south, and west of the center within each plot of the study area. Litter was removed and the soil samples were air-dried, ground, and analyzed for C and N concentrations using the combustion method at the University of Guelph's Agriculture and Food Laboratory. Total C consisted of both organic and inorganic C fractions.

### *2.3 Final Outlook*

The first objective of our study was to determine the environmental drivers of species richness within red pine plantation ecosystems. While light availability normally facilitates the growth and establishment of diverse understory flora, it may not benefit species richness in areas with thick red pine litter layers, which exhibit strong allelopathy effects that inhibit seedling emergence (Facelli et al., 1991; Montgomery & Chazdon, 2001). Local topography may also influence species composition by affecting microclimatic conditions, particularly through its impact on soil moisture and nutrient pools via leaching (Svenning, 2001). We used multiple regression analysis, with the Chao1 index as the primary response variable and $PPFD_U$, LAI, and TWI as predictor variables. Specifically, we conducted Type III analysis of variance (ANOVA) on the fitted linear models to assess whether each continuous environmental factor contributed significantly to observed variation in Chao1 richness. Multicollinearity among predictors was assessed using variance inflation factor, while the relationship between TWI and soil C and N was analysed separately (Zuur et al., 2010). We used a two-tailed t-test to estimate significance levels between all comparisons.

The second objective of our study was to evaluate the effects of VRH treatments on $PPFD_U$, LAI, TWI, and Chao1 species richness. VRH is known to help facilitate ecosystem resilience and heterogeneity in mixedwood forests. Although previous studies of our site point to light availability, litter input, and soil drainage changes, we aim to investigate how these manifest across different VRH treatments and affect species diversity in single-layered monocultures like red pine plantations (David B. Lindenmayer & Franklin, 2002). We used one-way ANOVA to test for significant differences in abiotic determinants and species richness between VRH treatments and types. Post-hoc comparisons were conducted for significant results using Tukey's Honest Significant Difference test to identify specific pairwise differences (Michael Kutner et al., 2004).

Through our study, we hope to contribute to the growing body of evidence on the ecological impacts of structural retention strategies. While VRH methods are often assumed to encourage environmental conditions that enhance understory species richness, we predict that this effect is context-dependent, and certain stands, such as red pine monocultures, carry unique surface litter dynamics and topographic features. These conditions may negate these benefits or further diminish biodiversity (Franklin et al., 2018; So et al., 2024). Looking forward, we recommend further research into targeted microsite amelioration, such as mechanical litter disturbance or nutrient amendments, in VRH and other management pathways to better support conservation in stands experiencing ongoing biodiversity loss.

**References**

Arain, M. A., Xu, B., Brodeur, J. J., Khomik, M., Peichl, M., Beamesderfer, E., Restrepo-Couple, N., & Thorne, R. (2022). Heat and drought impact on carbon exchange in an age-sequence of temperate pine forests. *Ecol Process*, *11*(1), 7. https://doi.org/10.1186/s13717-021-00349-7

Barakat, R. M. (2017). *A Comparison of Aboveground Biomass Estimates from Different Allometric Formulas using Vegetation Sampling Protocol in Rouge National Urban Park* University of Toronto]. https://api.semanticscholar.org/CorpusID:133198325

Beven, K. J., & Kirkby, M. J. (1979). A physically based, variable contributing area model of basin hydrology / Un modèle à base physique de zone d'appel variable de l'hydrologie du bassin versant. *Hydrological Sciences Bulletin*, *24*(1), 43-69. https://doi.org/10.1080/02626667909491834

Bodo, A. V., & Arain, M. A. (2022). Effects of variable retention harvesting on canopy transpiration in a red pine plantation forest. *Ecol Process*, *11*(1), 28. https://doi.org/10.1186/s13717-022-00366-0

Bodo, A. V., Parker, W. C., Elliott, K. A., & Arain, M. A. (2023). Below canopy evapotranspiration in four different variable retention harvesting treatments in a red pine plantation forest. *Hydrological Processes*, *37*(1). https://doi.org/10.1002/hyp.14789

Boucher, Y., Auger, I., Arseneault, D., Elzein, T., & Sirois, L. (2021). Long-term (1925–2015) forest structure reorganization in an actively managed temperate-boreal forest region of eastern North America. *Forest Ecology and Management*, *481*. https://doi.org/10.1016/j.foreco.2020.118744

Boyden, S., Montgomery, R., Reich, P. B., & Palik, B. (2012). Seeing the forest for the heterogeneous trees: stand-scale resource distributions emerge from tree-scale structure. *Ecol Appl*, *22*(5), 1578-1588. https://doi.org/10.1890/11-1469.1

Brandt, M., Tucker, C. J., Kariryaa, A., Rasmussen, K., Abel, C., Small, J., Chave, J., Rasmussen, L. V., Hiernaux, P., Diouf, A. A., Kergoat, L., Mertz, O., Igel, C., Gieseke, F., Schoning, J., Li, S., Melocik, K., Meyer, J., Sinno, S., . . . Fensholt, R. (2020). An unexpectedly large count of trees in the West African Sahara and Sahel. *Nature*, *587*(7832), 78-82. https://doi.org/10.1038/s41586-020-2824-5

Chao, A., Jost, L., & Chisholm, R. (2015). Estimating diversity and entropy profiles via discovery rates of new species. *Methods in Ecology and Evolution*, *6*(8), 873-882. https://doi.org/10.1111/2041-210x.12349

Dalponte, M., & Coomes, D. A. (2016). Tree-centric mapping of forest carbon density from airborne laser scanning and hyperspectral data. *Methods Ecol Evol*, *7*(10), 1236-1245. https://doi.org/10.1111/2041-210X.12575

David B. Lindenmayer, & Franklin, J. F. (2002). *Conserving Forest Biodiversity: A Comprehensive Multiscaled Approach*. Island Press.

Deng, J., Fang, S., Fang, X., Jin, Y., Kuang, Y., Lin, F., Liu, J., Ma, J., Nie, Y., Ouyang, S., Ren, J., Tie, L., Tang, S., Tan, X., Wang, X., Fan, Z., Wang, Q. W., Wang, H., & Liu, C. (2023). Forest understory vegetation study: current status and future trends. *For Res (Fayettev)*, *3*, 6. https://doi.org/10.48130/FR-2023-0006

Facelli, J. M., Pickett, S. T. A., & Facelli, J. M. (1991). Indirect Effects of Litter on Woody Seedlings Subject to Herb Competition. *Oikos*, *62*(2). https://doi.org/10.2307/3545257

Falkowski, M. J., Smith, A. M. S., Hudak, A. T., Gessler, P. E., Vierling, L. A., & Crookston, N. L. (2014). Automated estimation of individual conifer tree height and crown diameter via two-dimensional spatial wavelet analysis of lidar data. *Canadian Journal of Remote Sensing*, *32*(2), 153-161. https://doi.org/10.5589/m06-005

Franklin, C. M. A., Macdonald, S. E., & Nielsen, S. E. (2018). Combining aggregated and dispersed tree retention harvesting for conservation of vascular plant communities. *Ecol Appl*, *28*(7), 1830-1840. https://doi.org/10.1002/eap.1774

Franklin, C. M. A., Nielsen, S. E., & Macdonald, S. E. (2019). Understory vascular plant responses to retention harvesting with and without prescribed fire. *Canadian Journal of Forest Research*, *49*(9), 1087-1100. https://doi.org/10.1139/cjfr-2018-0288

Freudenberg, M., Magdon, P., & Nölke, N. (2022). Individual tree crown delineation in high-resolution remote sensing images based on U-Net. *Neural Computing and Applications*, *34*(24), 22197-22207. https://doi.org/10.1007/s00521-022-07640-4

Garber, S. M., Monserud, R. A., & Maguire, D. A. (2008). Crown Recession Patterns in Three Conifer Species of the Northern Rocky Mountains. *Forest Science*, *54*(6), 633-646. https://doi.org/10.1093/forestscience/54.6.633

Gatziolis, D., Fried, J. S., & Monleon, V. S. (2010). Challenges to Estimating Tree Height via LiDAR in Closed-Canopy Forests: A Parable from Western Oregon. *Forest Science*, *56*(2), 139-155. https://doi.org/10.1093/forestscience/56.2.139

Gering, L. R., & May, D. M. (1995). The Relationship of Diameter at Breast Height and Crown Diameter for Four Species Groups in Hardin County, Tennessee. *Southern Journal of Applied Forestry*, *19*(4), 177-181. https://doi.org/10.1093/sjaf/19.4.177

Gonsamo, A., & Chen, J. M. (2011). Evaluation of the GLC2000 and NALC2005 land cover products for LAI retrieval over Canada. *Canadian Journal of Remote Sensing*, *37*(3), 302-313. https://doi.org/10.5589/m11-039

Gonsamo, A., Walter, J.-M. N., & Pellikka, P. (2011). CIMES: A package of programs for determining canopy geometry and solar radiation regimes through hemispherical photographs. *Computers and Electronics in Agriculture*, *79*(2), 207-215. https://doi.org/10.1016/j.compag.2011.10.001

Gustafsson, L., Bauhus, J., Asbeck, T., Augustynczik, A. L. D., Basile, M., Frey, J., Gutzat, F., Hanewinkel, M., Helbach, J., Jonker, M., Knuff, A., Messier, C., Penner, J., Pyttel, P., Reif, A., Storch, F., Winiger, N., Winkel, G., Yousefpour, R., & Storch, I. (2020). Retention as an integrated biodiversity conservation approach for continuous-cover forestry in Europe. *Ambio*, *49*(1), 85-97. https://doi.org/10.1007/s13280-019-01190-1

Hao, Z., Lin, L., Post, C. J., Mikhailova, E. A., Li, M., Chen, Y., Yu, K., & Liu, J. (2021). Automated tree-crown and height detection in a young forest plantation using mask region-based convolutional neural network (Mask R-CNN). *ISPRS Journal of Photogrammetry and Remote Sensing*, *178*, 112-123. https://doi.org/10.1016/j.isprsjprs.2021.06.003

He, Q., Chen, E., An, R., & Li, Y. (2013). Above-Ground Biomass and Biomass Components Estimation Using LiDAR Data in a Coniferous Forest. *Forests*, *4*(4), 984-1002. https://doi.org/10.3390/f4040984

Hemery, G. E., Savill, P. S., & Pryor, S. N. (2005). Applications of the crown diameter–stem diameter relationship for different species of broadleaved trees. *Forest Ecology and Management*, *215*(1-3), 285-294. https://doi.org/10.1016/j.foreco.2005.05.016

Hu, B., & Jung, W. (2021). Individual Tree Crown Delineation from High Spatial Resolution Imagery Using U-Net. *The International Archives of the Photogrammetry, Remote Sensing and Spatial Information Sciences*, *XLIII-B3-2021*, 61-66. https://doi.org/10.5194/isprs-archives-XLIII-B3-2021-61-2021

Hu, B., Li, J., Jing, L., & Judah, A. (2014). Improving the efficiency and accuracy of individual tree crown delineation from high-density LiDAR data. *International Journal of Applied Earth Observation and Geoinformation*, *26*, 145-155. https://doi.org/10.1016/j.jag.2013.06.003

Iglhaut, J., Cabo, C., Puliti, S., Piermattei, L., O'Connor, J., & Rosette, J. (2019). Structure from Motion Photogrammetry in Forestry: a Review. *Current Forestry Reports*, *5*(3), 155-168. https://doi.org/10.1007/s40725-019-00094-3

Jonckheere, I., Nackaerts, K., Muys, B., & Coppin, P. (2005). Assessment of automatic gap fraction estimation of forests from digital hemispherical photography. *Agricultural and Forest Meteorology*, *132*(1-2), 96-114. https://doi.org/10.1016/j.agrformet.2005.06.003

Jucker, T., Fischer, F. J., Chave, J., Coomes, D. A., Caspersen, J., Ali, A., Loubota Panzou, G. J., Feldpausch, T. R., Falster, D., Usoltsev, V. A., Adu-Bredu, S., Alves, L. F., Aminpour, M., Angoboy, I. B., Anten, N. P. R., Antin, C., Askari, Y., Munoz, R., Ayyappan, N., . . . Zavala, M. A. (2022). Tallo: A global tree allometry and crown architecture database. *Glob Chang Biol*, *28*(17), 5254-5268. https://doi.org/10.1111/gcb.16302

Kanninen, M., Pérez, D., Montero, M., & Víquez, E. (2004). Intensity and timing of the first thinning of Tectona grandis plantations in Costa Rica: results of a thinning trial. *Forest Ecology and Management*, *203*(1-3), 89-99. https://doi.org/10.1016/j.foreco.2004.07.054

Kato-Noguchi, H., Kimura, F., Ohno, O., & Suenaga, K. (2017). Involvement of allelopathy in inhibition of understory growth in red pine forests. *J Plant Physiol*, *218*, 66-73. https://doi.org/10.1016/j.jplph.2017.07.006

Kim, M., Lee, W.-K., Kim, Y.-S., Lim, C.-H., Song, C., Park, T., Son, Y., & Son, Y.-M. (2015). Impact of thinning intensity on the diameter and height growth ofLarix kaempferistands in central Korea. *Forest Science and Technology*, *12*(2), 77-87. https://doi.org/10.1080/21580103.2015.1075435

Kim, S. R., Kwak, D. A., Lee, W. K., Son, Y., Bae, S. W., Kim, C., & Yoo, S. (2010). Estimation of carbon storage based on individual tree detection in Pinus densiflora stands using a fusion of aerial photography and LiDAR data. *Sci China Life Sci*, *53*(7), 885-897. https://doi.org/10.1007/s11427-010-4017-1

Kutchartt, E., Gayoso, J., Guerra, J., Pirotti, F., Castagneri, D., Matula, R., Rojas, Y., Olson, M. E., & Zwanzig, M. (2024). Shrub aboveground biomass estimation considering bulk volume geometry: general and specific models for 14 species in the Mediterranean central Chile. *New Forests*, *56*(1). https://doi.org/10.1007/s11056-024-10081-7

Lambert, M. C., Ung, C. H., & Raulier, F. (2005). Canadian national tree aboveground biomass equations. *Canadian Journal of Forest Research*, *35*(8), 1996-2018. https://doi.org/10.1139/x05-112

Leckie, D. (2003). Stand delineation and composition estimation using semi-automated individual tree crown analysis. *Remote Sensing of Environment*, *85*(3), 355-369. https://doi.org/10.1016/s0034-4257(03)00013-0

Lisiewicz, M. a. K., Agnieszka and Stereńczak, Krzysztof. (2022). Influence of the correction method of CHM−based Individual Tree Detection results on the estimation of forest stand characteristics. *Sylwan*, *166*, 362-377. https://doi.org/10.26202/sylwan.2022040

Martin, M. E., Newman, S. D., Aber, J. D., & Congalton, R. G. (1998). Determining Forest Species Composition Using High Spectral Resolution Remote Sensing Data. *Remote Sensing of Environment*, *65*(3), 249-254. https://doi.org/10.1016/s0034-4257(98)00035-2

Martire, S., Castellani, V., & Sala, S. (2015). Carrying capacity assessment of forest resources: Enhancing environmental sustainability in energy production at local scale. *Resources, Conservation and Recycling*, *94*, 11-20. https://doi.org/10.1016/j.resconrec.2014.11.002

Michael Kutner, Christopher Nachtsheim, John Neter, & Li, W. (2004). *Applied Linear Statistical Models* (5th ed.). McGraw-Hill/Irwin.

Molina, E., Valeria, O., De Grandpre, L., Ramirez, J. A., Cyr, D., & Boulanger, Y. (2021). Projecting future aboveground biomass and productivity of managed eastern Canadian mixedwood boreal forest in response to climate change. *Forest Ecology and Management*, *487*. https://doi.org/10.1016/j.foreco.2021.119016

Montgomery, R. A., & Chazdon, R. L. (2001). Forest Structure, Canopy Architecture, and Light Transmittance in Tropical Wet Forests. *Ecology*, *82*(10), 2707-2718. https://doi.org/10.1890/0012-9658(2001)082[2707:Fscaal]2.0.Co;2

Neeraj Kumar, Peter N. Belhumeur, Arijit Biswas, David W. Jacobs, W. John Kress, Ida C. Lopez, & Soares, J. V. B. (2012). *Leafsnap: A Computer Vision System for Automatic Plant Species Identification* Computer Vision – ECCV 2012

Ni-Meister, W., Lee, S., Strahler, A. H., Woodcock, C. E., Schaaf, C., Yao, T., Ranson, K. J., Sun, G., & Blair, J. B. (2010). Assessing general relationships between aboveground biomass and vegetation structure parameters for improved carbon estimate from lidar remote sensing. *Journal of Geophysical Research: Biogeosciences, 115*(G2). https://doi.org/10.1029/2009jg000936

Nyamai, P. A., Goebel, P. C., Gregory Corace, R., & Hix, D. M. (2020). Regeneration patterns of key pine species in a mixed-pine forest indicate a positive effect of variable retention harvesting and an increase in recruitment with time. *Forest Ecosystems*, *7*(1). https://doi.org/10.1186/s40663-020-00264-x

Panagiotidis, D., Abdollahnejad, A., Surový, P., & Chiteculo, V. (2016). Determining tree height and crown diameter from high-resolution UAV imagery. *International Journal of Remote Sensing*, *38*(8-10), 2392-2410. https://doi.org/10.1080/01431161.2016.1264028

Pappas, C., Bélanger, N., Bergeron, Y., Blarquez, O., Chen, H. Y. H., Comeau, P. G., De Grandpré, L., Delagrange, S., DesRochers, A., Diochon, A., D'Orangeville, L., Drapeau, P., Duchesne, L., Filotas, E., Gennaretti, F., Houle, D., Lafleur, B., Langor, D., Lebel Desrosiers, S., . . . Kneeshaw, D. (2022). Smartforests Canada: A Network of Monitoring Plots for Forest Management Under Environmental Change. In *Climate-Smart Forestry in Mountain Regions* (pp. 521-543). https://doi.org/10.1007/978-3-030-80767-2_16

Qi, R. C. a. S., Hao and Kaichun, Mo and Guibas, Leonidas J. (2017). PointNet: Deep Learning on Point Sets for 3D Classification and Segmentation. 2017 IEEE Conference on Computer Vision and Pattern Recognition (CVPR),

Richard Dickinson, & Royer, F. (2014). *Plants of Southern Ontario, Trees, Shrubs, Wildflowers, Grasses, Ferns and Aquatic Plants*. Lone Pine Publishing.

Rupp, H., Tauchnitz, N., & Meissner, R. (2021). The Effects of Soil Drying Out and Rewetting on Nitrogen and Carbon Leaching—Results of a Long-Term Lysimeter Experiment. *Water*, *13*(18). https://doi.org/10.3390/w13182601

Russell, M. B., Weiskittel, A. R., & Kershaw, J. A. (2014). Comparing strategies for modeling individual-tree height and height-to-crown base increment in mixed-species Acadian forests of northeastern North America. *European Journal of Forest Research*, *133*(6), 1121-1135. https://doi.org/10.1007/s10342-014-0827-1

So, K., Rogers, C. A., Li, Y., Arain, M. A., & Gonsamo, A. (2024). Retention forestry as a climate solution: Assessing biomass, soil carbon and albedo impacts in a northern temperate coniferous forest. *Sci Total Environ*, *947*, 174680. https://doi.org/10.1016/j.scitotenv.2024.174680

Sothe, C., Gonsamo, A., Arabian, J., Kurz, W. A., Finkelstein, S. A., & Snider, J. (2022). Large Soil Carbon Storage in Terrestrial Ecosystems of Canada. *Global Biogeochemical Cycles*, *36*(2). https://doi.org/10.1029/2021gb007213

Spitale, S. P. (2011). *Succession in the Understory of Red Pine Plantations in Southern Ontario* University of Waterloo]. University of Waterloo. http://hdl.handle.net/10012/6421

Svenning, J.-C. (2001). On the role of microenvironmental heterogeneity in the ecology and diversification of neotropical rain-forest palms (Arecaceae). *The Botanical Review*, *67*(1), 1-53. https://doi.org/10.1007/bf02857848

Van Deusen, P. C., & Heath, L. S. (2010). Weighted analysis methods for mapped plot forest inventory data: Tables, regressions, maps and graphs. *Forest Ecology and Management*, *260*(9), 1607-1612. https://doi.org/10.1016/j.foreco.2010.08.010

Wan Mohd Jaafar, W. S., Woodhouse, I. H., Silva, C. A., Omar, H., Abdul Maulud, K. N., Hudak, A. T., Klauberg, C., Cardil, A., & Mohan, M. (2018). Improving Individual Tree Crown Delineation and Attributes Estimation of Tropical Forests Using Airborne LiDAR Data. *Forests*, *9*(12). https://doi.org/10.3390/f9120759

Weinstein, B. G., Marconi, S., Aubry-Kientz, M., Vincent, G., Senyondo, H., White, E. P., & Record, S. (2020). DeepForest: A Python package for RGB deep learning tree crown delineation. *Methods in Ecology and Evolution*, *11*(12), 1743-1751. https://doi.org/10.1111/2041-210x.13472

Weinstein, B. G., Marconi, S., Bohlman, S., Zare, A., & White, E. (2019). Individual Tree-Crown Detection in RGB Imagery Using Semi-Supervised Deep Learning Neural Networks. *Remote Sensing*, *11*(11). https://doi.org/10.3390/rs11111309

Westfall, J. A. (2012). A Comparison of Above-Ground Dry-Biomass Estimators for Trees in the Northeastern United States. *Northern Journal of Applied Forestry*, *29*(1), 26-34. https://doi.org/10.5849/njaf.11-001

White, J. C., Coops, N. C., Wulder, M. A., Vastaranta, M., Hilker, T., & Tompalski, P. (2016). Remote Sensing Technologies for Enhancing Forest Inventories: A Review. *Canadian Journal of Remote Sensing*, *42*(5), 619-641. https://doi.org/10.1080/07038992.2016.1207484

Wielgosz, M., Puliti, S., Xiang, B., Schindler, K., & Astrup, R. (2024). SegmentAnyTree: A sensor and platform agnostic deep learning model for tree segmentation using laser scanning data. *Remote Sensing of Environment*, *313*. https://doi.org/10.1016/j.rse.2024.114367

Wu, B., Yu, B., Wu, Q., Huang, Y., Chen, Z., & Wu, J. (2016). Individual tree crown delineation using localized contour tree method and airborne LiDAR data in coniferous forests. *International Journal of Applied Earth Observation and Geoinformation*, *52*, 82-94. https://doi.org/10.1016/j.jag.2016.06.003

Xu, D., Wang, H., Xu, W., Luan, Z., & Xu, X. (2021). LiDAR Applications to Estimate Forest Biomass at Individual Tree Scale: Opportunities, Challenges and Future Perspectives. *Forests*, *12*(5). https://doi.org/10.3390/f12050550

Yin, D., & Wang, L. (2019). Individual mangrove tree measurement using UAV-based LiDAR data: Possibilities and challenges. *Remote Sensing of Environment*, *223*, 34-49. https://doi.org/10.1016/j.rse.2018.12.034

Yun, T., Jiang, K., Li, G., Eichhorn, M. P., Fan, J., Liu, F., Chen, B., An, F., & Cao, L. (2021). Individual tree crown segmentation from airborne LiDAR data using a novel Gaussian filter and energy function minimization-based approach. *Remote Sensing of Environment*, *256*. https://doi.org/10.1016/j.rse.2021.112307

Zhu, G., Zhou, L., He, X., Wei, P., Lin, D., Qian, S., Zhao, L., Luo, M., Yin, X., Zeng, L., Long, Y., Hu, S., Ouyang, X., & Yang, Y. (2022). Effects of Elevation Gradient on Soil Carbon and Nitrogen in a Typical Karst Region of Chongqing, Southwest China. *Journal of Geophysical Research: Biogeosciences*, *127*(6). https://doi.org/10.1029/2021jg006742

Zugic, J. I., Pisaric, M. F. J., McKenzie, S. M., Parker, W. C., Elliott, K. A., & Arain, M. A. (2021). The Impact of Variable Retention Harvesting on Growth and Carbon Sequestration of a Red Pine (Pinus resinosa Ait.) Plantation Forest in Southern Ontario, Canada. *Frontiers in Forests and Global Change*, *4*. https://doi.org/10.3389/ffgc.2021.725890

Zuur, A. F., Ieno, E. N., & Elphick, C. S. (2010). A protocol for data exploration to avoid common statistical problems. *Methods in Ecology and Evolution*, *1*(1), 3-14. https://doi.org/10.1111/j.2041-210X.2009.00001.x